

Escaped and Trapped Emission of Organic Light-Emitting Diodes

This content has been downloaded from IOPscience. Please scroll down to see the full text.

2012 Chinese Phys. Lett. 29 024209

(<http://iopscience.iop.org/0256-307X/29/2/024209>)

View [the table of contents for this issue](#), or go to the [journal homepage](#) for more

Download details:

IP Address: 202.117.17.90

This content was downloaded on 18/12/2016 at 09:07

Please note that [terms and conditions apply](#).

You may also be interested in:

[Optical Interference Effects by Metal Cathode in OrganicLight-Emitting Diodes](#)

Wu Zhao-Xin, Wang Li-Duo and Qiu Yong

[Frustrated total internal reflection in organic light-emitting diodes employing sphere cavity embedded in polystyrene](#)

Peifen Zhu

[Improved light extraction of organic light emitting diodes with a nanopillar patterning structure](#)

Gao Zhi-Xiang, Wang Hua, Hao Yu-Ying et al.

[Improvement in the light outcoupling efficiency of organic light-emitting diodes using a hemispherical lens and a multipatterned one-dimensional photonic crystal fabricated by autocloning](#)

Hiroshi Fujimoto, Masayuki Yahiro, Takayuki Kawashima et al.

[Horizontal Orientation of a Linear-Shaped Platinum\(II\) Complex in Organic Light-Emitting Diodes with a High Light Out-Coupling Efficiency](#)

Masatsugu Taneda, Takuma Yasuda and Chihaya Adachi

[High ambient contrast ratio OLED and QLED without a circular polarizer](#)

Guanjun Tan, Ruidong Zhu, Yi-Shou Tsai et al.

[High efficiency quantum dot and organic LEDs with a back-cavity and a high index substrate](#)

Haowen Liang, Zhenyue Luo, Ruidong Zhu et al.

[Device optimization of tris-aluminum \(Alq3\) based bilayer organic light emitting diode structures](#)

J Chan, A D Raki, C Y Kwong et al.

Escaped and Trapped Emission of Organic Light-Emitting Diodes

LIANG Shi-Xiong(梁士雄), WU Zhao-Xin(吴朝新)**, ZHAO Xuan-Ke(赵选科), HOU Xun(侯洵)

Key Laboratory of Photonics Technology for Information, Key Laboratory for Physical Electronics and Devices (Ministry of Education), School of Electronic and Information Engineering, Xi'an Jiaotong University, Xi'an 710049

(Received 9 October 2011)

By locating the emitters around the first and second antinode of the metal electrode, the escaped and trapped emission of small molecule based bottom emission organic light-emitting diodes is investigated by using an integrating sphere, a fiber spectrometer and a glass hemisphere. It is found that the external coupling ratio by locating the emitters at the second antinode (at a distance of 220 nm from the cathode) is 70%, which is higher than that of an emitter at the first antinode (60 nm from the cathode) in theory and experiment. Extending the “half-space” dipole model by taking the dipole radiation pattern into account, we also calculate the optical coupling efficiency for the emitter at both the first and second antinode. Our experimental and theoretical results will benefit the optimization of device structures for the higher out-coupling efficiency.

PACS: 42.25.Bs, 42.25.Hz, 42.70.Jk, 42.79.Gn

DOI:10.1088/0256-307X/29/2/024209

Organic light emitting devices (OLEDs) have received a great deal of attention in recent years due to their potential application in flat panel displays and lighting.^[1] Although an internal quantum efficiency of nearly 100% has been achieved,^[2,3] due to the mismatch of the refractive index of air, glass substrate, and organic layer, a great deal of the generated light is lost through total internal reflection into the substrate and indium-tin-oxide (ITO) wave-guiding modes, and to self-absorption ultimately. Thus the outcoupling efficiency (η_{ext}) is a critical figure for OLEDs. The η_{ext} is calculated by classical ray optics to be $1/2n^2$, where n is the refractive index of substrate^[4] For glass substrate ($n = 1.52$), the calculated external coupling efficiency is about 20%. Due to the amazing theoretical optical loss, a number of methods have been developed to enhance the external coupling efficiency. For example, substrate modifications that enable extraction the light in the glass substrate,^[5–8] the ordered micro-lens arrays,^[9–12] and the diffusive layer,^[13–16] and microcavities^[17] were used to increase the external coupling efficiency. However, the above-mentioned methods only achieved an efficiency enhancement of from 22% to 56%, and there is still no general consensus on extracting trapped light. In fact, the emitters are optically close to the highly reactive metal cathode, the optical emission properties of OLEDs are strongly modified by the optical interference between the reflective electric field and the dipole radiated fields.^[18–20] We can change the spectrum and the emission intensity by adjusting the locations of emitters. Therefore, optimal efficiency of OLEDs can also be achieved by locating emitters around the antinode condition of metal cathode. For general OLEDs, the emitters are located at the first antinode, due to the low conductivity and low carrier mobility of organic materials. When the emitters are located at the sec-

ond antinode,^[21,22] there are some different characteristics due to the interference effect.

In this study, an integrating sphere, a fiber spectrometer and a glass hemisphere are used to experimentally investigate the light outcoupling characters of OLEDs when locating the emitters around the first and second antinode of the metal electrode. Furthermore, we extend the “half-space” dipole model by taking the dipole radiation pattern into account. It is found that light outcoupling efficiency of OLEDs can be enhanced by locating emitters around the second antinode, but more light may be coupled into the ITO/Organic waveguiding modes at the second antinode.

The OLED structure used in both experiment and modeling is shown in Fig. 1(a). On the glass substrate, the indium-tin-oxide (ITO) layer is used as anode ($n_{\text{ITO}} \approx 1.9$, thickness 100 nm). A layer of 4,4', 4''-tris(3-methylphenylphenylamino) triphenylamine (m-MTDATA) doped with 1.5wt% of tetrafluorotetracyano-quinodimethane (F4-TCNQ) is spin coated on ITO as the p-doped hole-injection layer.^[23] We also made different thickness of this layer by using various spin speeds and varying concentrations of solutions; then, an N,N'-bis(1-naphthyl)-N,N'-diphenyl-1,1'-biphenyl-4,4'-diamine (NPB) with a thickness of 20 nm is evaporation deposited as a hole transport layer, and a tris-8-hydroxyquinoline aluminum (Alq3, $n_{\text{Alq3}} = 1.72$) layer is evaporation deposited as the electron transportation and emitting layer; the thicknesses of Alq3 for different devices are 30 nm, 60 nm, 90 nm, 120 nm, 150 nm, 180 nm, 200 nm, 220 nm, 240 nm, 260 nm. The 0.8-nm-thick LiF and 80-nm-thick Al is evaporation deposited as the cathode of OLEDs. The glass substrates are 33 mm × 44 mm, 30 mm × 37 mm, 27 mm × 32 mm or 25 mm × 26 mm, the thickness is

**Corresponding author. Email: zhaoxinwu@mail.xjtu.edu.cn

© 2012 Chinese Physical Society and IOP Publishing Ltd

1.2 mm, the four emission areas all are $3\text{ mm} \times 4\text{ mm}$, and the emission area is at the center of the device. The dimensions of the device are shown in Fig. 1(b). Details of the fabrication processes can be found in our previous publications.^[24]

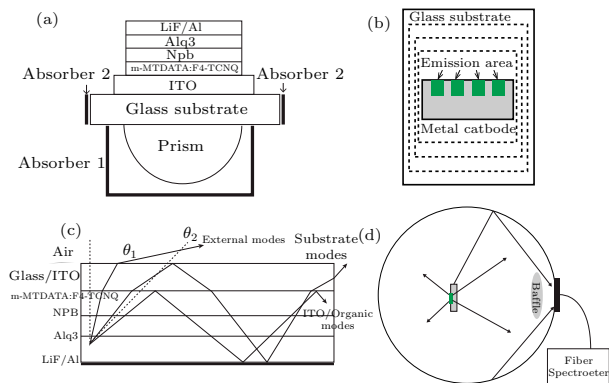


Fig. 1. (a) Schematic diagrams of the structures of OLEDs and measurement methods; (b) the dimensions profile of the device, the dashed lines are the profiles of the other three substrates; (c) schematic diagram showing photons emitted into various modes; (d) schematic diagram of the integrating sphere and fiber spectrometer measurement system.

The optical structure of the device is shown in Fig. 1(c). The emission layer is bounded by the metal cathode and the ITO-glass substrate with an interface to air. Due to the total internal reflection, we can divide the emission light into three modes by their corresponding angular ranges, namely, the extracted modes, substrate modes, and ITO/organic modes. A detailed description can be found in our previous publications.^[20,25]

Then the external coupling efficiency can be defined as $\eta_{\text{ext}} = \text{extracted modes} / (\text{extracted modes} + \text{substrate modes} + \text{ITO/organic modes})$.

In fact, the absorption coefficient of ITO is on the order of 5000 cm^{-1} ,^[26] so the ITO/organic modes can not be detected from the edges. A part of the substrate modes are absorbed by the OLED when zigzagging to the substrate edges, so the measured value of this modes is underestimated and should be corrected to obtain the real value. Then the η_{ext} can not be measured directly, and only the external coupling ratio r_{ext} can be directly obtained to be $r_{\text{ext}} = \text{extracted modes} / (\text{extracted modes} + \text{correctional substrate modes})$.

In the previous reports,^[27–29] silicon photodiode (or silicon photodiode arrays) and charge coupled device spectrographs are the most widely used detectors for the electroluminescence (EL) measurements of OLEDs. This can only detect the discrete emission intensity at a given angle, and the discrete values were added to obtain the total photon flux. One could not directly obtain the flux, and this easily induces measurement errors. In our research, the photon

flux of devices was measured by using an integrating sphere (SLM-12, Sphere Optics LLC) combined with a fiber spectrometer (USB 2000⁺, Ocean Optics Inc.), as shown in Fig. 1(d). The diameter of the integrating sphere is 250 cm, which is much greater than the size of the emitting area, and the dimension is suitable for decreasing the instrumental error. A glass hemisphere is also used in our measurement, which can extract almost all of the substrate modes into external coupling modes. A similar measurement method is also used in other works.^[30–33] The fiber spectrometer features high sensitivity, stable quantum efficiency over a certain wavelength range, and near-linear response with the incident light power. The integrating sphere can collect all of the light emitted from the OLED.

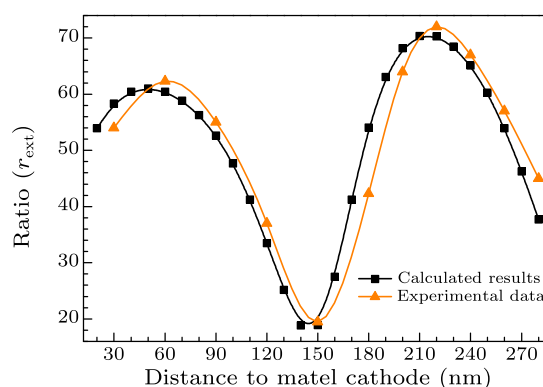


Fig. 2. The measured and calculated external coupling ratios.

In order to measure the external modes and substrate modes, we used absorber 1 and absorber 2, as shown in Fig. 1(a). Firstly, the prepared OLED with the edges of the substrate was covered by absorber 2 (Fig. 1(a)), and it was lit under a given voltage and current, then the measured flux F_1 is external coupling modes. Secondly, with the emitting areas covered by a glass hemisphere, we obtained the total optical output flux F_{TOT} . Thirdly, the edges of the substrate were covered by absorber 2, and the emitting area was still covered by the glass hemisphere, then the measured flux F'_1 is the sum of the external modes F_{surf} and the extracted substrate modes F_{edge} ; Fourthly, with the emitting areas covered by the glass hemisphere and absorber 1, the flux F_2 is the sum of un-extracted substrate modes, F'_{edge} , and ITO/Organic modes $F_{\text{ITO/org}}$. Lastly, absorber 2, absorber 3 and a hemisphere prism all were covered on all edges and surface of the substrate, and then, the flux F_3 of ITO/organic modes ($F_{\text{ITO/org}}$) could be obtained. An index-matching fluid is applied between the hemisphere and the OLEDs, with the same refractive index as the glass substrate, to ensure proper optical contact. In the five steps, the OLED was lit under the same current density (r_{ext} does not change with current density), and the measurement is rapidly

accomplished, so the attenuation of devices is negligible.

The absorption coefficient of ITO and organic material is of the order of magnitude of 5000 cm^{-1} ,^[26] so the light of the ITO/organic modes can almost not escape the layers before dissipation, and $F_3 \approx 0$. The absorption of the glass substrate at the wavelength of about 520 nm is very low, and the light is several reflected at the metal cathode surface when zigzagging to the substrate edges, the metal cathode absorbs about 14% of energy at once reflection. The reflection times are calculated by the formula $N = D/2d \tan \theta$, where D is the width of the Al cathode, d is the thickness of the glass substrate ($d=1.2 \text{ mm}$), and θ is the light emission angle. Thus the real value of the unextracted substrate modes (F'_2) can be obtained by retrieving the absorption of metal cathode and glass, and the total flux of the external coupling modes and substrate modes is ($F'_1 + F'_2$). Then, the external coupling ratio r_{ext} , as shown in Fig. 2, is calculated by the equation

$$r_{\text{ext}} = F_1/(F'_1 + F'_2). \quad (1)$$

The fluxes of the total emission, the extracted modes, substrate modes all are obtained by our measurement. The measured external coupling ratio r_{ext} is calculated by Eq. (1). The r_{ext} is from 20% to 70%, which varies with the thickness of Alq₃, and there is about 5% measurement error. After the first measurement, we change the glass substrate size to $30 \text{ mm} \times 37 \text{ mm}$, $27 \text{ mm} \times 32 \text{ mm}$, $25 \text{ mm} \times 26 \text{ mm}$ (Fig. 1(c)), the emission areas do not change, and we remeasure the devices. The results do not alter, so the substrate size does not affect the value of r_{ext} . The r_{ext} almost does not affect by different thickness of m-MTDATA:F4-TCNQ.

From the experimental data in Fig. 2, the r_{ext} of emitters at the antinodes is surely higher than those at other positions, and the external coupling ratio by locating emitters at the second antinodes is 16% higher than the first antinode. In order to accurately investigate the r_{ext} , we also extended the half-space dipole model.^[27] by taking the dipole radiation pattern into account. In fact, the emission of a dipole is not isotropic; its spatial radiation intensity varies with the emission angle.^[34] In our model, the emission of the organic layer is considered as an oscillating dipole emission in front of a mirror.^[35] This emission layer is Alq₃ for our devices. These dipoles are embedded inside the emitter half space at a distance z from the mirror (Al cathode-reflector in Fig. 1(a)). The other half space is occupied by the Al cathode. The emission of a dipole is anisotropic, so these dipoles should be divided into three freedoms for calculation, as shown in Fig. 3. This model is also able to represent the interference between the directly emitted light and the light reflected by the metal cathode. Then, we cal-

culate the angular distribution of the radiation intensity, and then extract the external coupling ratio. In OLEDs, the energy coupled to surface plasmon modes is by the near field effect of dipoles,^[36,37] so it is non-radioactive loss, and it does not alter the emission patterns of OLEDs. Thus in our model, we do not take the surface plasmon loss into account.

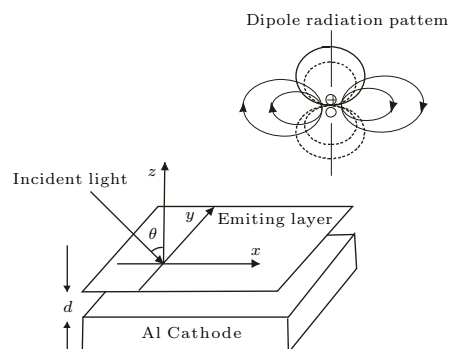


Fig. 3. The schematic diagram of the extended half-space dipole model and the radiation pattern of the dipole (on the top right corner).

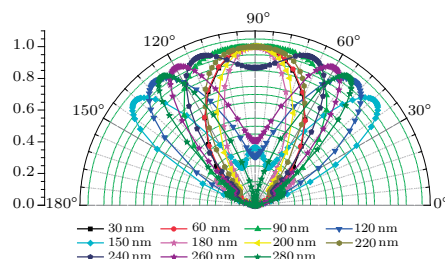


Fig. 4. The calculated and normalized internal angular emission distributions patterns.

As shown in Fig. 3, for the emitting dipoles, the angular distribution of emission intensity I can be written as^[35]

$$I(\theta) = E_1^2 |1 + r_p \exp(2i\delta \cos \theta)|^2 + E_2^2 |1 - r_p \exp(2i\delta \cos \theta)|^2 + E_3^2 |1 + r_s \exp(2i\delta \cos \theta)|^2, \quad (2)$$

where r_s and r_p is the Fresnel reflection coefficient for the s- and p-polarizations, θ is the internal emission angle with respect to the direction of the Poynting vector, δ is the phase change incurring in the round trip from the emitter to the organic/cathode interface and back, and $\delta = 2\pi nd/\lambda_0$ with λ_0 being the emission center wavelength in vacuum, n the refractive index of organic layer and d the distance from the emitters to the interface of metal cathode and organic layers. At the xoy plane, the angular distribution of the emission intensity of the three kinds of dipoles are calculated by $E_1 = P_e \sin \theta / 4\pi \epsilon r^3$, $E_2 = P_e \cos \theta / 4\pi \epsilon r^3$, and $E_3 = P_e / 4\pi \epsilon r^3$,^[34] where E is the angular distribution of oscillating dipole emitting, and P_e is the electric dipole moment, which is constant for a fixed dipole, ϵ is the dielectric constant of the organic layer,

and r is the distance from the dipole from a certain point.

The curves in Fig. 4 describe the calculated internal angular emission distribution patterns, which change with distances from the cathode rapidly, due to the interference effect. We also calculate the external angular emission distribution patterns of OLEDs, and the external intensity angular distribution at the first antinode is much more isotropic than that at the second antinode. This characteristic is useful for display and luminance applications.

In order to exactly calculate the photon flux of various modes, the light intensity $I(\theta)$ is integrated at each angle range of the three modes (i.e., $\int_{\text{angle range}} 2\pi \sin \theta I(\theta) d\theta$), and the photon flux of the various modes is obtained. Figure 5 illustrates the calculated percentage of the three kinds of modes, and the external coupling efficiency η_{ext} at different distances from the metal cathode. The η_{ext} is 57% and 61% at the first and second antinodes, respectively. When the distance is 150 nm, the η_{ext} is 13%, namely only 14% of the light escapes the device, and most of the light is trapped in the device as ITO/organic waveguiding modes. Furthermore, the external coupling ratio r_{ext} can also be calculated, as shown in Fig. 2, taking the range of r_{ext} from 20% to 70% at different distances from the metal cathode. Our study will benefit the optimization of device structures for higher out-coupling efficiency.

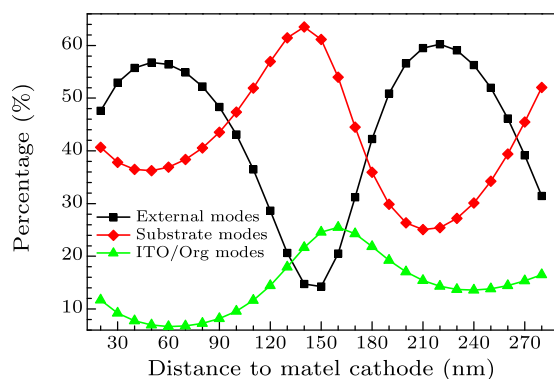


Fig. 5. The calculated percentage of the three kinds of modes, namely substrate modes, external modes, ITO/organic modes for different distances from the metal cathode.

In conclusion, an integrating sphere associating with a fiber spectrometer and hemisphere measurement and an extend half-space dipole model have been developed to describe the external coupling ratio of OLEDs. It is found that the external coupling ratio by locating emitters at the second antinode is 70%, which is higher than that of the emitter at the first antinode. The internal angular emission distribution patterns are also calculated. The numerical results are in good agreement with our experiments. These

results will benefit researchers to optimize the structure of small molecule based bottom emitting devices.

References

- [1] Forrest S R 2003 *Org. Electron.* **4** 45
- [2] Adachi C, Baldo M A, Thompson M E and Forrest S R 2001 *J. Appl. Phys.* **90** 5048
- [3] Tong B H, Mei Q B, Wang S J, Fang Y, Meng Y Z and Wang B 2008 *J. Mater. Chem.* **18** 1636
- [4] Greenham N C, Friend R H and Bradley D D C 1994 *Adv. Mater.* **6** 491
- [5] Chen S M and Kwok H S 2010 *Opt. Express* **18** 37
- [6] Madigan C F, Lu M H and Sturm J C 2000 *Appl. Phys. Lett.* **76** 1650
- [7] Ziebarth J M, Saafir A K, Fan S and McGehee M D 2004 *Adv. Funct. Mater.* **14** 451
- [8] Cheng Y H, Wu J L, Cheng C H, Syao K C and Lee M C M 2007 *Appl. Phys. Lett.* **90** 3
- [9] Moller S and Forrest S R 2002 *J. Appl. Phys.* **91** 3324
- [10] Wei M K and Su I L 2004 *Opt. Express* **12** 5777
- [11] Yamasaki T, Sumioka K and Tsutsui T 2000 *Appl. Phys. Lett.* **76** 1243
- [12] Li F, Li X, Zhang J and Yang B 2007 *Org. Electron.* **8** 635
- [13] Nakamura T, Tsutsumi N, Juni N and Fujii H 2004 *J. Appl. Phys.* **96** 6016
- [14] Shiang J J and Duggal A R 2004 *J. Appl. Phys.* **95** 2880
- [15] Bathelt R, Buchhauser D, Garditz C, Paetzold R and Wellmann P 2007 *Org. Electron.* **8** 293
- [16] Riedel B, Shen Y X, Hauss J, Aichholz M, Tang X C, Lemmer U and Gerken M 2011 *Adv. Mater.* **23** 740
- [17] Lemmer U, Hennig R, Guss W, Ochse A, Pommerehne J, Sander R, Greiner A, Mahrt R F, Bassler H, Feldmann J and Gobel E O 1995 *Appl. Phys. Lett.* **66** 1301
- [18] So S K, Choi W K, Leung L M and Neyts K 1999 *Appl. Phys. Lett.* **74** 1939
- [19] Wan W M V, Greenham N C and Friend R H 2000 *J. Appl. Phys.* **87** 2542
- [20] Wu Z X, Wang L D and Qiu Y 2004 *Chin. Phys. Lett.* **21** 1370
- [21] Lin C L, Cho T Y, Chang C H and Wu C C 2006 *Appl. Phys. Lett.* **88** 081114
- [22] Kim S Y and Kim J J 2010 *Org. Electron.* **11** 1010
- [23] Zhou X, Pfeiffer M, Blochwitz J, Werner A, Nollau A and Fritz T, Leo K 2001 *Appl. Phys. Lett.* **78** 410
- [24] Wu Z X, Wang L, Li G T and Qiu Y 2005 *J. Appl. Phys.* **97** 103105
- [25] Liang, S X, Wu Z X, Zhao X K, Wang D W and Hou X 2010 *Proc. SPIE* **7852** 785200
- [26] Kim J S, Ho P K H, Thomas D S, Friend R H, Cacialli F, Bao G W and Li S F Y 1999 *Chem. Phys. Lett.* **315** 307
- [27] Kim J S, Ho P K H, Greenham N C and Friend R H 2000 *J. Appl. Phys.* **88** 1073
- [28] Bulovic V, Khalfin V B, Gu G, Burrows P E, Garbuzov D Z and Forrest S R 1998 *Phys. Rev. B* **58** 3730
- [29] Lu M H and Sturm J C 2002 *J. Appl. Phys.* **91** 595
- [30] deMello J C, Wittmann H F and Friend R H 1997 *Adv. Mater.* **9** 230
- [31] He Y, Hattori R and Kanicki J 2000 *Rev. Sci. Instrum.* **71** 2104
- [32] Hong Y T and Kanicki J 2003 *Rev. Sci. Instrum.* **74** 3572
- [33] Van M S L M, Carvelli M, Megens M, Wehenkel D, Bartyzel M, Greiner H, Janssen R A J and Coehoorn R 2010 *Nature Photon.* **4** 329
- [34] Stratton J A 1941 *Electromagnetic Theory* (New York: McGraw-Hill)
- [35] Bjork G 1994 *IEEE J. Quantum Electron.* **30** 2314
- [36] Hobson P A, Wasey J A E, Sage I and Barnes W L 2002 *IEEE J. Sel. Top. Quantum Electron.* **8** 378